

A Brief Overview of Plate Finite Element Methods

C. Lovadina

Università di Pavia, Italy; carlo.lovadina@unipv.it

25.1 Introduction

In this chapter we present a brief account of possible finite element methods (FEMs) for the plate bending problem, when described by means of the *Reissner–Mindlin* model. We point out that the following overview is *far from being exhaustive*: we are perfectly aware that many important approaches are not even mentioned. Accordingly, also the references are very limited and lack completeness.

The choice of schemes that are going to be described is strongly biased by the author’s experience, and it does not correspond to any efficiency or robustness criterion. We also remark that we are not going to detail any *rigorous* convergence and stability proof. Rather, we will try to heuristically explain

1. the main troubles arising from the FEM discretization of plate problems (Section 25.2);
2. why the methods under consideration succeed in the solution approximation (Section 25.3).

25.2 The Reissner–Mindlin Plate Model and Its FEM Discretization

25.2.1 The Reissner–Mindlin Plate Model

The Reissner–Mindlin equations for a clamped plate with a convex mid-plane domain Ω require us to find (θ, w) such that (see, for example, [Ba95] or [Hu87])

$$\begin{cases} -\operatorname{div} \mathbf{C}\varepsilon(\theta) - \lambda t^{-2}(\nabla w - \theta) = 0 & \text{in } \Omega, \\ -\operatorname{div} (\lambda t^{-2}(\nabla w - \theta)) = g & \text{in } \Omega, \\ \theta = 0, w = 0 & \text{on } \partial\Omega. \end{cases} \quad (25.1)$$

In (25.1), t is the plate thickness, λ is the shear modulus, and \mathbf{C} is the tensor of bending moduli, given (for isotropic materials) by

$$\mathbf{C}\tau := \frac{E}{12(1-\nu^2)}[(1-\nu)\tau + \nu \operatorname{tr}(\tau)\mathbf{I}], \quad (25.2)$$

where τ is a generic second-order symmetric tensor, $\operatorname{tr}(\tau)$ its trace, \mathbf{I} is the second-order identity tensor, and E and ν are the Young modulus and Poisson ratio, respectively. Moreover, $\theta = (\theta_1, \theta_2)$ represents the (vector) rotation field and w is the transversal displacement (see Figure 25.1), while g is a given transversal load. Finally, ∇ is the usual symmetric gradient operator.

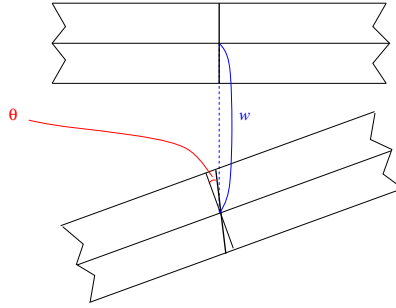


Fig. 25.1. Reissner–Mindlin kinematic variables.

Introducing the space $\Theta \times W = (H_0^1(\Omega))^2 \times H_0^1(\Omega)$, it is easily seen that problem (25.1) can be reformulated as the following *minimization* problem over $\Theta \times W$ for the elastic energy E_t :

$$\begin{cases} \text{Find } (\theta, w) \in \Theta \times W \text{ which minimizes} \\ E_t(\eta, v) := \frac{1}{2} \int_{\Omega} \mathbf{C}\varepsilon(\eta) : \varepsilon(\eta) + \frac{\lambda t^{-2}}{2} \int_{\Omega} |\nabla v - \eta|^2 - \int_{\Omega} gv. \end{cases} \quad (25.3)$$

From a mechanical viewpoint, the term $\frac{1}{2} \int_{\Omega} \mathbf{C}\varepsilon(\eta) : \varepsilon(\eta)$ represents the bending energy, the term $\frac{\lambda t^{-2}}{2} \int_{\Omega} |\nabla v - \eta|^2$ gives the shear energy, and $\int_{\Omega} gv$ is the external load work. A standard computation leads to the Euler–Lagrange equations associated with problem (25.3):

$$\begin{cases} \text{Find } (\theta, w) \in \Theta \times W \text{ such that} \\ \int_{\Omega} \mathbf{C}\varepsilon(\theta) : \varepsilon(\eta) + \lambda t^{-2} \int_{\Omega} (\nabla w - \theta) \cdot (\nabla v - \eta) = \int_{\Omega} gv \end{cases} \quad (25.4)$$

for every $(\eta, v) \in \Theta \times W$. We remark that, for every fixed $t > 0$, the bilinear form

$$\int_{\Omega} \mathbf{C}\varepsilon(\theta) : \varepsilon(\eta) + \lambda t^{-2} \int_{\Omega} (\nabla w - \theta) \cdot (\nabla v - \eta)$$

is *continuous, symmetric, and coercive* over $\Theta \times W$. Moreover, for g smooth, $v \rightarrow \int_{\Omega} gv$ is a *linear and continuous functional* over W . Therefore, problem (25.4) is elliptic and the Lax–Milgram lemma implies the existence, uniqueness, and stability of its solution.

The ellipticity of the problem suggests to consider Galerkin discretization techniques for the solution approximation. Among them, the FEM is a very popular and flexible choice (see, for example, [Ci78]). We briefly recall that a *conforming* finite element procedure for our plate problem is based on the following steps.

- *Mesh generation.* Construct a decomposition \mathcal{T}_h of Ω into triangular elements T . The mesh size h , defined as the maximum diameter of all the triangles in the decomposition, is an important geometric parameter. The mesh is typically required to fulfill some compatibility conditions. A typical mesh is displayed in Figure 25.2. We also remark that quadrilateral elements may be used as well.

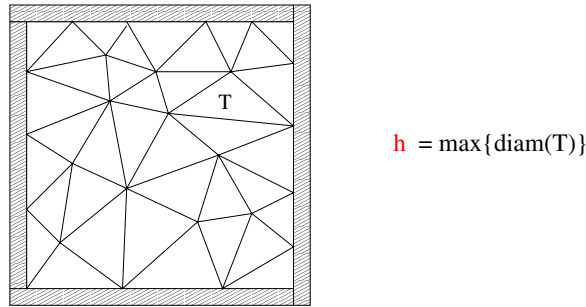


Fig. 25.2. A typical triangular mesh.

- *Local approximation.* For each T in the mesh \mathcal{T}_h , introduce $P(T)$, a polynomial space on T . Different choices for different elements may be made. However, the most common choice consists of selecting the same shape functions for every element.
- *Finite element space.* Form the *discrete space*

$$\Theta_h \times W_h = \{(\eta_h, v_h) \in \Theta \times W : (\eta_h, v_h)|_T \in P(T)\}.$$

For instance, one could select piecewise linear and globally continuous functions for both rotations and vertical displacements. This choice is schematically depicted in Figure 25.3. Here the bullets mean that the relevant unknown is uniquely determined by assigning the values at the triangle vertices.

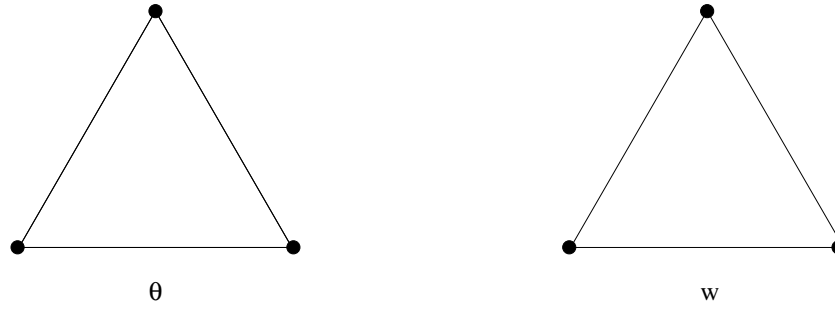


Fig. 25.3. The simplest FEM space.

- *Discrete problem.* Solve the problem

$$\begin{cases} \text{Find } (\theta_h, w_h) \in \Theta_h \times W_h \text{ s.t.} \\ \int_{\Omega} \mathbf{C}\varepsilon(\theta_h) : \varepsilon(\eta_h) + \lambda t^{-2} \int_{\Omega} (\nabla w_h - \theta_h) \cdot (\nabla v_h - \eta_h) = \int_{\Omega} g v_h \end{cases} \quad (25.5)$$

for every $(\eta_h, v_h) \in \Theta_h \times W_h$.

25.2.2 Locking Effects and Spurious Mode Occurrence

Since the problem is elliptic for each $t > 0$, the standard theory gives optimal error estimates for the discrete solution $(\theta_h, w_h) \in \Theta_h \times W_h$, as the mesh size tends to zero (see [Ci78] or [BrFo91], for instance). In practice, this means that reasonable outcomes are expected when using a mesh as in Figure 25.2, and the approximation spaces as in Figure 25.3. However, for a “small” thickness the discrete solution heavily underestimates the analytical solution (see Figure 25.4 for a pictorial representation of this occurrence, when the plate is clamped and subjected to a constant load).

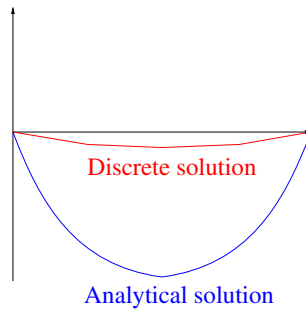


Fig. 25.4. Typical locking solution.

To understand this bad phenomenon, known as the *shear locking effect* (see, e.g., [BrFo91]), it is worth considering the asymptotic behavior of the problem as $t \rightarrow 0$. More precisely, it can be proved that problem (25.3) converges, in a suitable sense, to the *limit constrained problem* (see, for example, [SaPa92] or [ChPa94])

$$\begin{cases} \text{Find } (\theta^0, w^0) \in K \text{ which minimizes} \\ E_0(\eta, v) = \frac{1}{2} \int_{\Omega} \mathbf{C}\varepsilon(\eta) : \varepsilon(\eta) - \int_{\Omega} gv, \quad (\eta, v) \in K, \end{cases} \quad (25.6)$$

where K is defined by

$$K = \{(\eta, v) \in \Theta \times W : \nabla v = \eta\}. \quad (25.7)$$

Even though we will not detail the convergence proof, we point out that the constraint $(\theta^0, w^0) \in K$ is very reasonable. Indeed, in minimizing the functional $E_t(\cdot, \cdot)$ in (25.3) for *very small* t , one should choose functions (η, v) such that

$$\int_{\Omega} |\nabla v - \eta|^2 \text{ is "very small" (which means } \nabla v - \eta \text{ is "very small");}$$

otherwise, one pays an enormous amount of shear energy in the term

$$\frac{\lambda t^{-2}}{2} \int_{\Omega} |\nabla v - \eta|^2.$$

We also remark that problem (25.6) is coercive and continuous on K . Furthermore, K is a *non-trivial* closed subspace of $\Theta \times W$. Indeed, given *any* compactly supported smooth function v , one may set $\eta := \nabla v$. By construction, $(\eta, v) \in K$. Therefore, the *continuous limit* problem (25.6) may be thought of as a standard well-posed (elliptic) problem.

We now turn our attention to the discrete problem. The discrete problem (25.5) is equivalent to a minimization problem for the *same* functional $E_t(\cdot, \cdot)$ (see (25.3)), but restricted to $\Theta_h \times W_h$, i.e.,

$$\begin{cases} \text{Find } (\theta_h, w_h) \in \Theta_h \times W_h \text{ which minimizes} \\ E_t(\eta_h, v_h) := \frac{1}{2} \int_{\Omega} \mathbf{C}\varepsilon(\eta_h) : \varepsilon(\eta_h) + \frac{\lambda t^{-2}}{2} \int_{\Omega} |\nabla v_h - \eta_h|^2 - \int_{\Omega} gv_h. \end{cases} \quad (25.8)$$

Therefore, the FEM problem converges, as $t \rightarrow 0$, to the discrete limit problem

$$\begin{cases} \text{Find } (\theta_h^0, w_h^0) \in K_h \text{ which minimizes} \\ E_0(\eta_h, v_h) = \frac{1}{2} \int_{\Omega} \mathbf{C}\varepsilon(\eta_h) : \varepsilon(\eta_h) - \int_{\Omega} gv_h, \quad (\eta_h, v_h) \in K_h, \end{cases} \quad (25.9)$$

where

$$K_h = \{(\eta_h, v_h) \in \Theta_h \times W_h : \nabla v_h = \eta_h\} = K \cap (\Theta_h \times W_h). \quad (25.10)$$

We remark that the discrete limit problem accounts for minimizing the same limit functional as for the continuous problem (see (25.6)), but this time on the discrete subspace K_h .

Let us analyze the structure of K_h , when using piecewise linear and globally continuous functions (see Figure 25.3). If $(\eta_h, v_h) \in K_h$, then $\nabla v_h = \eta_h$ (see (25.10)). Since $\eta_h \in C^0(\Omega)$, we deduce that $v_h \in C^1(\Omega)$. But v_h is also piecewise linear, so $v_h \in C^1(\Omega)$ implies that v_h is a *globally linear function* in Ω . If the plate is clamped on a part of the boundary of positive length, we then infer that $v_h = 0$. Recalling that $\eta_h = \nabla v_h$, we finally deduce that

$$(\eta_h, v_h) \in \Theta_h \times W_h \implies (\eta_h, v_h) = (0, 0),$$

i.e., $K_h = \{(0, 0)\}$. Therefore, the limit problem (25.9) is just a minimization problem for a “good” functional, but on a *trivial* space: the minimizing pair is surely $(\theta_h, w_h) = (0, 0)$!

Of course, this is the limit “zero thickness” situation; however, for a “small thickness” (with respect to the mesh size h), the discrete problem is essentially so close to the limit case that the discrete solution is very small: *shear locking* has occurred.

Since the trouble stands in the shear energy term, a possible cure consists in reducing, somehow, its influence at the discrete level. This can be accomplished by considering the *modified* energy

$$E_{h,t}(\eta_h, v_h) = \frac{1}{2} \int_{\Omega} \mathbf{C}\varepsilon(\eta_h) : \varepsilon(\eta_h) + \frac{\lambda t^{-2}}{2} \int_{\Omega} |R_h(\nabla v_h - \eta_h)|^2 - \int_{\Omega} g v_h,$$

where R_h is a suitable *reduction* operator. Therefore, the finite element scheme now reads, in its equivalent minimization formulation,

$$\left\{ \begin{array}{l} \text{Find } (\theta_h, w_h) \in \Theta_h \times W_h \text{ which minimizes} \\ E_{h,t}(\eta_h, v_h) := \frac{1}{2} \int_{\Omega} \mathbf{C}\varepsilon(\eta_h) : \varepsilon(\eta_h) + \frac{\lambda t^{-2}}{2} \int_{\Omega} |R_h(\nabla v_h - \eta_h)|^2 - \int_{\Omega} g v_h. \end{array} \right. \quad (25.11)$$

As $t \rightarrow 0$, the problem will consequently converge to the problem

$$\left\{ \begin{array}{l} \text{Find } (\theta_h^0, w_h^0) \in K_h \text{ which minimizes} \\ E_{h,0}(\eta_h, v_h) = \frac{1}{2} \int_{\Omega} \mathbf{C}\varepsilon(\eta_h) : \varepsilon(\eta_h) - \int_{\Omega} g v_h, \quad (\eta_h, v_h) \in K_h, \end{array} \right. \quad (25.12)$$

where K_h is now defined by

$$K_h = \{(\eta_h, v_h) \in \Theta_h \times W_h : R_h(\nabla v_h - \eta_h) = 0\}. \quad (25.13)$$

We point out that now the constraint has been relaxed to $R_h(\nabla v_h - \eta_h) = 0$, and we don't have $\nabla v_h - \eta_h = 0$ anymore. As a consequence, one may hope

that K is large enough to properly approximate the subspace K (see (25.7)), thus preventing shear locking effects. However, the reduction operator R_h must be carefully selected. Let us consider the following (not recommended) choice.

For the approximation space $\Theta_h \times W_h$, we select piecewise quadratic and globally continuous functions, as schematically depicted in Figure 25.5.

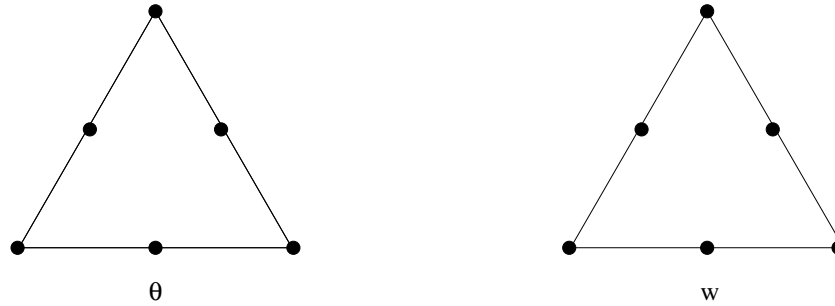


Fig. 25.5. Quadratic approximation.

We choose R_h as the L^2 -projection operator onto the piecewise constant (vector-valued) functions. It can be proved that there is $v_h^* \in W_h$ for which $\nabla v_h^* \neq 0$ but $R_h(\nabla v_h^*) = 0$. Computing the energy $E_{h,t}(\cdot, \cdot)$ along the direction given by $(0, v_h^*) \in \Theta_h \times W_h$, we get (see (25.11))

$$E_h(\alpha(0, v_h^*)) = \frac{\lambda t^{-2}}{2} \int_{\Omega} |\alpha R_h(\nabla v_h^*)|^2 - \alpha \int_{\Omega} g v_h^* = -\alpha \int_{\Omega} g v_h^* \quad \forall \alpha \in \mathbb{R}.$$

Therefore, the functional $E_{h,t}(\cdot, \cdot)$ is *linear* along that particular direction. As a consequence, no minimizing pair $(\theta_h, w_h^*) \in \Theta_h \times W_h$ can be found, since ellipticity has been lost at the discrete level. From a practical point of view, one obtains a *singular* stiffness matrix. Of course, this is an extreme situation. However, even when the stiffness matrix is invertible, a naive choice of the reduction operator R_h may lead to a milder, though nasty, phenomenon: the occurrence of *spurious modes*, i.e., the discrete solution exhibits non-physical heavy oscillations.

Obviously, to avoid the existence of $v_h^* \in W_h$ such that $\nabla v_h^* \neq 0$ but $R_h(\nabla v_h^*) = 0$, one would like to choose $R_h = Id$, the identity operator. However, this choice will lead to trouble, again with the shear locking.

To summarize, we need to reduce the influence of the shear energy term, but

- If R_h reduces “too much,” we risk *spurious modes* occurrence.
- If R_h does not reduce “enough,” we risk *shear locking* effects.

Balancing R_h is not a trivial task. However, nowadays there are several efficient options in the literature. Some of them are briefly reviewed in the following section.

25.3 Some Efficient Finite Element Techniques

25.3.1 MITC Elements

We now describe one of the most popular and efficient strategies to approximate the solution of the Reissner–Mindlin plate equations: the so-called Mixed Interpolation of Tensorial Components (*MITC*) elements (see [BBF89], [BFS91], but also [TeHu85] and [Du92], for example). We here focus on a particular low-order element, but higher-order, as well as quadrilateral versions, are available. The scheme under consideration, known as the *MITC7* element, consists in making the following choice.

- To approximate each rotational component, we select piecewise quadratic and globally continuous functions. In addition, a local cubic bubble is inserted.
- To approximate the vertical displacements, we select piecewise quadratic and globally continuous functions.

To complete the element description, we need to specify the reduction operator R_h . To this end, for each triangle T we introduce the vectorial space

$$\Gamma(T) := (P_1(T))^2 + P_1(T)(y, -x)^T,$$

where $P_1(T)$ denotes the space of linear functions on T . It can be proved that a function in $\Gamma(T)$ is uniquely determined by assigning

- the moments up to the first order of its tangential component, for each edge of T (6 degrees of freedom);
- its mean value over T (2 degrees of freedom).

For a given smooth vectorial function $\delta = (\delta_1, \delta_2)$, we then define $R_h\delta$ by requiring that

$$\left\{ \begin{array}{l} (R_h\delta)|_T \in \Gamma(T), \\ \int_T R_h\delta = \int_T \delta, \\ \int_e [(R_h\delta) \cdot \mathbf{t}] p_1(s) ds = \int_e [\delta \cdot \mathbf{t}] p_1(s) ds, \end{array} \right. \quad (25.14)$$

for every triangle $T \in \mathcal{T}_h$, and every edge e of T . Above, \mathbf{t} is the tangent vector to the side e , while $p_1(s)$ is a linear polynomial with respect to a local

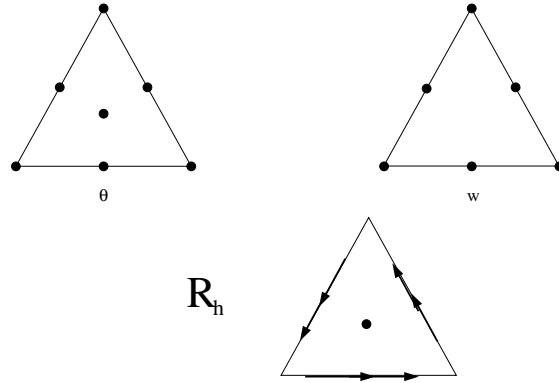


Fig. 25.6. The MITC7 element.

coordinate s along e . All these choices and definitions are schematically shown in Figure 25.6.

The MITC7 element, as well as all the other schemes based on the MITC philosophy, is carefully designed to fulfill the following crucial features.

- **P1.** R_h is the identity operator when applied to the gradients of *discrete* vertical displacements, i.e.,

$$R_h \nabla v_h = \nabla v_h \quad \forall v_h \in W_h.$$

- **P2.** If $\text{curl } R_h \eta = 0$, then $R_h \eta$ is the gradient of a *discrete* vertical displacement, i.e.,

$$\{R_h \eta : \eta \in (H_0^1(\Omega))^2, \text{curl } R_h \eta = 0\} = \nabla W_h.$$

(Above and in what follows, the curl operator is defined as

$$\text{curl } \varphi = \partial \varphi_2 / \partial x - \partial \varphi_1 / \partial y,$$

for a generic vector-valued function $\varphi = (\varphi_1, \varphi_2)$.)

There exists an auxiliary space Q_h such that (for the MITC7 element, this space consists of the locally linear functions, with no continuity requirements across the element interfaces):

- **P3.** The “commutative diagram property”

$$\text{curl } R_h \eta = P_h \text{curl } \eta, \quad \eta \in (H_0^1(\Omega))^2,$$

holds, where $P_h : L^2 \rightarrow Q_h$ is the L^2 projection operator.

- **P4.** The pair of spaces (Θ_h, Q_h) is stable for Stokes-like problems.

We now comment on the properties above. We first notice that the very important property **P1** prevents the scheme from suffering from spurious modes.

To see which is the role played by the other properties, we focus on the *limit* problem, as $t \rightarrow 0$. As detailed in Section 25.2.2, this accounts for considering the problem (see (25.6)–(25.7)):

$$\begin{cases} \text{Find } (\theta^0, w^0) \in K \text{ which minimizes} \\ E_0(\eta, v) = \frac{1}{2} \int_{\Omega} \mathbf{C}\varepsilon(\eta) : \varepsilon(\eta) - \int_{\Omega} gv, \quad (\eta, v) \in K, \end{cases} \quad (25.15)$$

where

$$K = \{(\eta, v) \in \Theta \times W : \nabla v = \eta\}. \quad (25.16)$$

The discrete counterpart reads

$$\begin{cases} \text{Find } (\theta_h^0, w_h^0) \in K_h \text{ which minimizes} \\ E_0(\eta_h, v_h) = \frac{1}{2} \int_{\Omega} \mathbf{C}\varepsilon(\eta_h) : \varepsilon(\eta_h) - \int_{\Omega} gv_h \quad (\eta_h, v_h) \in K_h, \end{cases} \quad (25.17)$$

where

$$K_h = \{(\eta_h, v_h) \in \Theta_h \times W_h : \nabla v_h = R_h \eta_h\}. \quad (25.18)$$

Roughly speaking, problem (25.17) has a chance to be a “good approximation” of problem (25.15), for all loads g , only if K_h is a “good approximation” of K . This means that, given $(\eta, v) \in K$, we need to find $(\eta_I, v_I) \in K_h$ such that

$$\eta_I \approx \eta, \quad v_I \approx v. \quad (25.19)$$

Above, $\eta \approx \eta_I$ means that some suitable norm of $\eta - \eta_I$ vanishes as the mesh size h tends to zero. The same remark applies to $v_I \approx v$, of course.

If $(\eta, v) \in K$ is sufficiently regular, the most natural choice would be to take η_I and v_I as the usual Lagrange interpolants of η and v , respectively (if $(\eta, v) \in K$ is less regular, one might think of the Clément’s interpolants, see [Ci78]). Unfortunately, even though $\nabla v = \eta$, in general it is not true that the choice above leads to a (η_I, v_I) such that $\nabla v_I = R_h \eta_I$. Therefore, $(\eta_I, v_I) \notin K_h$, and a more sophisticated and subtle choice needs to be made, as sketched below.

Fix $(\eta, v) \in K$. We first consider the discretization of the Stokes-like problem:

$$\begin{cases} \text{Find } (\eta_I, p_h) \in \Theta_h \times Q_h \text{ such that} \\ \int_{\Omega} \mathbf{C}\varepsilon(\eta_I) : \varepsilon(\chi_h) + \int_{\Omega} p_h \operatorname{curl} \chi_h = \int_{\Omega} \mathbf{C}\varepsilon(\eta) : \varepsilon(\chi_h), \quad \chi_h \in \Theta_h, \\ \int_{\Omega} q_h \operatorname{curl} \eta_I = 0, \quad q_h \in Q_h. \end{cases} \quad (25.20)$$

From property **P4**, we deduce that

$$\eta_I \approx \eta, \quad P_h \operatorname{curl} \eta_I = 0. \quad (25.21)$$

Such a $\eta_I \in \Theta$ will be our approximation of $\eta \in \Theta$. We now need to construct a suitable $v_I \in W_h$. From (25.21) and property **P3** we get

$$\operatorname{curl} R_h \eta_I = P_h \operatorname{curl} \eta_I = 0. \quad (25.22)$$

Property **P2** then implies that there exists $v_I \in W_h$ such that

$$\nabla v_I = R_h \eta_I. \quad (25.23)$$

Therefore, it holds for $(\eta_I, v_I) \in K_h$. In addition, since it holds for $\eta_I \approx \eta$ (see (25.21)), it follows that

$$R_h \eta_I \approx \eta = \nabla v. \quad (25.24)$$

Since $R_h \eta_I = \nabla v_I$ (see (25.23)), from (25.24) we deduce that

$$\nabla v_I \approx \nabla v, \quad (25.25)$$

which implies that $v_I \approx v$.

To summarize, using properties **P1–P4**, we have been able to find, for a given $(\eta, v) \in K$, a pair $(\eta_I, v_I) \in K_h$ such that $(\eta_I, v_I) \approx (\eta, v)$. This heuristically explains why the *MITC* elements are efficient.

Coming back to property **P4**, we point out that the connection between the Reissner–Mindlin problem and a Stokes-like problem is much deeper. Indeed, introducing the *Helmholtz decomposition* for $\lambda t^{-2}(\nabla w - \theta)$, that is,

$$\lambda t^{-2}(\nabla w - \theta) = \nabla \varphi + \operatorname{curl} p, \quad \varphi \in H_0^1(\Omega) = W, \quad p \in H_0^1(\Omega)/\mathbb{R}, \quad (25.26)$$

the plate problem (25.4) can be rewritten in the equivalent form (see [BrFo86])

$$\left\{ \begin{array}{l} \text{Find } (\theta, w; \varphi, p) \in \Theta \times W \times W \times H_0^1(\Omega)/\mathbb{R} \text{ such that} \\ \int_{\Omega} \nabla \varphi \cdot \nabla v = \int_{\Omega} g v \quad \forall v \in W, \\ \int_{\Omega} \mathbf{C} \varepsilon(\theta) : \varepsilon(\eta) - \int_{\Omega} p \operatorname{curl} \eta = \int_{\Omega} \nabla \varphi \cdot \eta \quad \forall \eta \in \Theta, \\ - \int_{\Omega} q \operatorname{curl} \theta - \lambda^{-1} t^2 \int_{\Omega} \operatorname{curl} p \cdot \operatorname{curl} q = 0 \quad \forall q \in H_0^1(\Omega)/\mathbb{R}, \\ \int_{\Omega} \nabla w \cdot \nabla \psi = \int_{\Omega} \theta \cdot \nabla \psi + \lambda^{-1} t^2 \int_{\Omega} \nabla \varphi \cdot \nabla \psi \quad \forall \psi \in W. \end{array} \right. \quad (25.27)$$

Above and in what follows, the curl operator is defined as

$$\operatorname{curl} q = (\partial q / \partial y, -\partial q / \partial x)^T,$$

for a generic scalar function q . Problem (25.27) reveals that the Reissner–Mindlin plate problem can be decomposed into

1. An elliptic problem for φ (the first variational equation);
2. A singularly perturbed *Stokes-like problem* for (θ, p) (the second and the third variational equation);
3. Another elliptic problem for w (the fifth variational equation).

In light of this reformulation, it should not be surprising that a Reissner–Mindlin element may contain ingredients peculiar to the mixed finite element machinery for the Stokes problem approximation.

25.3.2 The Arnold–Falk Element

We now present a triangular scheme which heavily exploits formulation (25.27) for the plate problem: the Arnold–Falk element (see [ArFa89]). This element is based on the following choices.

- Θ_h : each component of the rotation field is approximated by means of piecewise linear and globally continuous functions. In addition, a local cubic bubble is inserted per each triangle in the mesh.
- W_h : the vertical displacements are approximated by means of locally linear functions, which are continuous across adjacent elements *at the edge mid-points* (called the *non-conforming P_1 element*). It is easily seen that this approximation field is obtained by assigning its values at the edge mid-points.

The element is schematically shown in Figure 25.7.

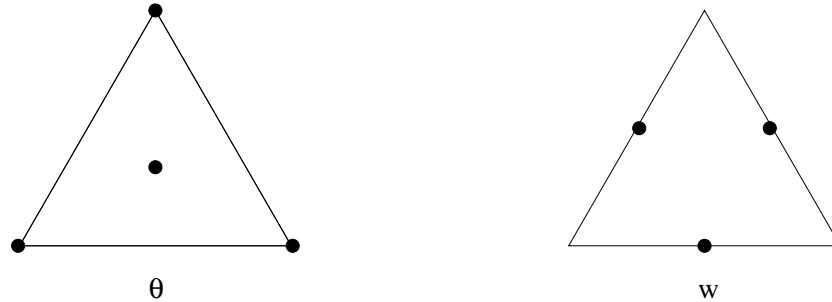


Fig. 25.7. The Arnold–Falk element.

Furthermore, we select R_h as P_0 , the projection operator on the piecewise constant functions. Introducing the element-wise gradient operator ∇_h , and noting that $P_0 \nabla_h v_h = \nabla v_h$ for any $v_h \in W_h$, the discrete problem then reads

$$\left\{ \begin{array}{l} \text{Find } (\theta_h, w_h) \in \Theta_h \times W_h \text{ which minimizes} \\ E_{h,t}(\eta_h, v_h) = \frac{1}{2} \int_{\Omega} \mathbf{C}\varepsilon(\eta_h) : \varepsilon(\eta_h) + \frac{\lambda t^{-2}}{2} \int_{\Omega} |\nabla_h v_h - P_0 \eta_h|^2 - \int_{\Omega} g v_h. \end{array} \right. \quad (25.28)$$

The key point is to recognize that the *piecewise constant function* $\lambda t^{-2} (\nabla_h w_h - P_0 \theta)$ admits a *discrete Helmholtz decomposition* (see (25.26)) as follows:

$$\lambda t^{-2} (\nabla_h w_h - R_h \theta) = \nabla_h \varphi_h + \text{curl } p_h, \quad \varphi_h \in W_h, \quad p_h \in Q_h, \quad (25.29)$$

where Q_h is the space of piecewise linear and globally continuous functions. The discretization spaces for φ_h and p_h are depicted in Figure 25.8.

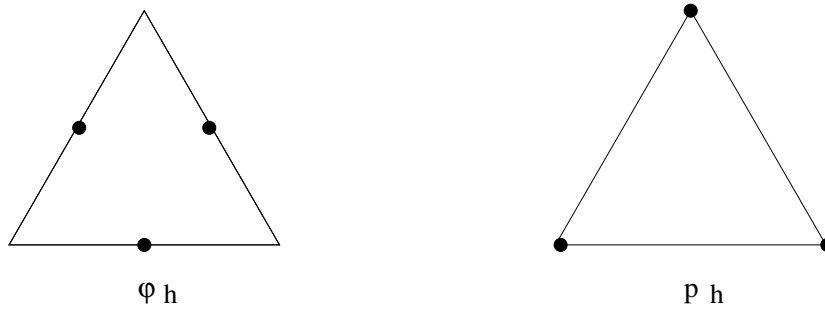


Fig. 25.8. Auxiliary spaces for the Arnold–Falk element.

Using that decomposition in the Euler–Lagrange equations emanated from problem (25.28), we get the variational system

$$\left\{ \begin{array}{l} \text{Find } (\theta_h, w_h; \varphi_h, p_h) \in \Theta_h \times W_h \times W_h \times Q_h \text{ such that} \\ \int_{\Omega} \nabla_h \varphi_h \cdot \nabla_h v_h = \int_{\Omega} g v_h, \\ \int_{\Omega} \mathbf{C}\varepsilon(\theta_h) : \varepsilon(\eta_h) - \int_{\Omega} p_h \text{curl } \eta_h = \int_{\Omega} \nabla_h \varphi_h \cdot \eta_h, \\ - \int_{\Omega} q_h \text{curl } \theta_h - \lambda^{-1} t^2 \int_{\Omega} \text{curl } p_h \cdot \text{curl } q_h = 0, \\ \int_{\Omega} \nabla_h w_h \cdot \nabla_h \psi_h = \int_{\Omega} \theta_h \cdot \nabla \psi_h + \lambda^{-1} t^2 \int_{\Omega} \nabla_h \varphi_h \cdot \nabla_h \psi_h, \end{array} \right. \quad (25.30)$$

for every $(\eta_h, v_h; \psi_h, q_h) \in \Theta_h \times W_h \times W_h \times Q_h$. Therefore, the Arnold–Falk scheme is equivalent to

1. Discretizing a Poisson problem by means of W_h , the space of non-conforming P_1 elements.

2. Discretizing a Stokes-like problem using the pair $\Theta \times Q_h$, which is the popular and stable *MINI element* (see [BrFo91], for instance).
3. Discretizing a further Poisson problem, still using W_h .

Since all the choices above are stable and convergent for the corresponding problems, the Arnold–Falk element results in a good approximation scheme for the Reissner–Mindlin plate problem.

25.3.3 Linked Interpolation Technique

We now describe a technique which has become quite popular, especially among the engineering community: the *linked interpolation technique* (see [AuTa94], [AuLo01], and [Lo98], for example). The main idea consists in improving the vertical displacements by using the rotational degrees of freedom. More precisely, the basic steps of this strategy are the following.

- Select finite element spaces Θ_h and W_h , as usual.
- Introduce a *suitable* linear operator (the *linking operator*)

$$L_h : \Theta_h \longrightarrow H_0^1(\Omega). \quad (25.31)$$

- Form the finite dimensional subspace of $\Theta \times W$:

$$X_h = \{(\eta_h, v_h^*) = (\eta_h, v_h + L_h \eta_h) : \eta_h \in \Theta_h, v_h \in W_h\}. \quad (25.32)$$

- Consider the discrete problem

$$\left\{ \begin{array}{l} \text{Find } (\theta_h, w_h^*) \in X_h \text{ which minimizes} \\ E_{h,t}(\eta_h, v_h^*) = \frac{1}{2} \int_{\Omega} \mathbf{C} \varepsilon(\eta_h) : \varepsilon(\eta_h) + \frac{\lambda t^{-2}}{2} \int_{\Omega} |P_h(\nabla v_h^* - \eta_h)|^2 \\ \qquad \qquad \qquad - \int_{\Omega} g v_h^*, \end{array} \right. \quad (25.33)$$

where P_h is typically a suitable L^2 -projection operator.

The role of the *linking operator* L_h should be to help relax the constraint which causes locking effects. To give an example, we consider a triangular low-order element which corresponds to the following choices (see Figure 25.9).

- Θ_h : each component of the rotation field is approximated by means of piecewise linear and globally continuous functions. In addition, a local cubic bubble is inserted per each triangle in the mesh.
- W_h : the vertical displacements are approximated by means of piecewise linear and globally continuous linear functions.

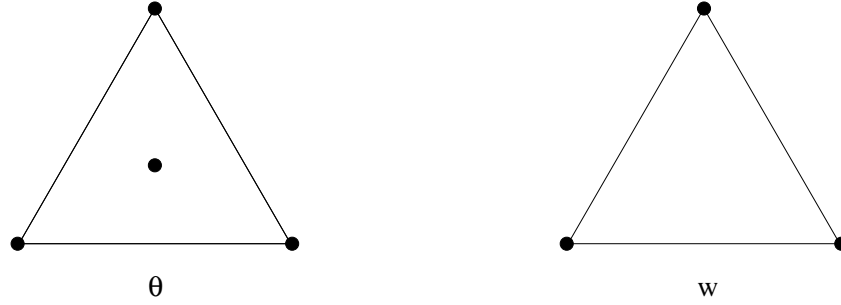


Fig. 25.9. Approximation of rotations and deflections for the lowest-order linked interpolation scheme.

The *linking operator* $L_h : \Theta_h \rightarrow H_0^1(\Omega)$ is defined as follows. For each $T \in \mathcal{T}_h$, we set

$$\varphi_i = \lambda_j \lambda_k \quad \text{and} \quad EB_2(T) = \text{Span} \{ \varphi_i \}_{1 \leq i \leq 3}, \tag{25.34}$$

where $\{ \lambda_i \}_{1 \leq i \leq 3}$ are the barycentric coordinates of the triangle T and the indices (i, j, k) form a permutation of the set $(1, 2, 3)$. Then, the operator L_h is locally defined as

$$L_h \eta_h|_T = \sum_{i=1}^3 \alpha_i \varphi_i \in EB_2(T), \tag{25.35}$$

where the coefficients α_i are determined by requiring that

$$(\nabla L_h \eta_h - \eta_h) \cdot \mathbf{t} \quad \text{is constant on each } e. \tag{25.36}$$

Above, \mathbf{t} denotes the tangential vector to the edge e . Therefore, a generic $v_h^* = v_h + L_h \eta_h$ (see (25.32)) is indeed a locally *quadratic* function. Finally, the operator P_h introduced in (25.33) is chosen as P_0 , the L^2 -projection operator over the piecewise constant functions.

The linked interpolation technique has some strong connections with the *MITC* elements described in Section 25.3.1. To see how this can occur, let us consider the term $\nabla v_h^* - \eta_h$ in (25.33). Recalling (25.32), we get

$$\nabla v_h^* - \eta_h = \nabla(v_h + L_h \eta_h) - \eta_h = \nabla v_h - [\eta_h - \nabla L_h \eta_h].$$

The vector $\eta_h - \nabla L_h \eta_h$ is often very similar (and sometimes even identical) to $R_h \eta_h$, where R_h is exactly the reduction operator of Section 25.3.1. For more details, the interested reader may see [Ly00].

25.3.4 PSRI Technique

The partial selective reduced integration (PSRI) technique is based on a suitable splitting of the shear energy term (see [ArBr93]). We illustrate the idea in

the easiest possible case: we first choose a real parameter α , with $0 < \alpha < t^{-2}$. We then introduce finite element spaces Θ_h and W_h , together with a reduction operator R_h . We finally consider the discrete problem:

$$\left\{ \begin{array}{l} \text{Find } (\theta_h, w_h) \in \Theta_h \times W_h \text{ which minimizes} \\ E_{h,t}(\eta_h, v_h) = \frac{1}{2} \int_{\Omega} \mathbf{C}\varepsilon(\eta_h) : \varepsilon(\eta_h) + \frac{\lambda\alpha}{2} \int_{\Omega} |(\nabla v_h - \eta_h)|^2 \\ \quad + \frac{\lambda(t^{-2} - \alpha)}{2} \int_{\Omega} |R_h(\nabla v_h - \eta_h)|^2 - \int_{\Omega} g v_h. \end{array} \right. \quad (25.37)$$

Therefore, the shear energy term has been split into two parts, the first of which is *exactly* integrated, while the second one is *reduced* by means of R_h . The advantage of this formulation stands in the fact that the term

$$\frac{1}{2} \int_{\Omega} \mathbf{C}\varepsilon(\eta_h) : \varepsilon(\eta_h) + \frac{\lambda\alpha}{2} \int_{\Omega} |(\nabla v_h - \eta_h)|^2$$

is *always coercive over the whole space* $\Theta \times W$. As a consequence, spurious modes cannot occur independently of the chosen Θ_h and W_h spaces. With respect to the original discrete formulation (25.11), we now have much more flexibility in the choice of the approximation spaces. For instance, we could now reconsider the following element (see [Lo96]).

- Θ_h and W_h : both rotations and vertical displacements are discretized by means of piecewise quadratic and globally continuous functions (see Figure 25.10).
- $R_h = P_0$, the L^2 -projection operator on the piecewise constant functions.

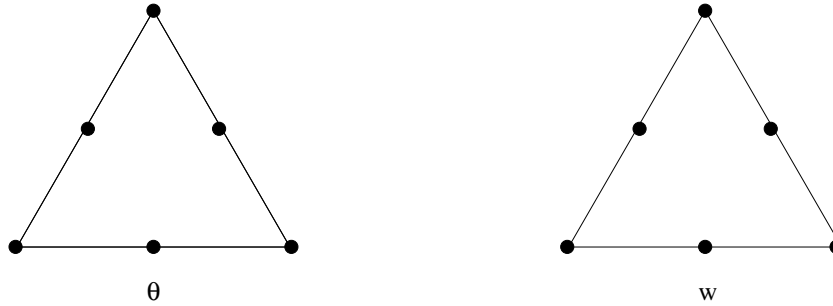


Fig. 25.10. Approximation of rotations and deflections for a low-order *PSRI* scheme.

This element shares the same degrees of freedom for all the kinematic variables, a feature which may be favorable for a possible extension to *shell* problems.

The main drawback of this approach is the presence of the parameter α to be chosen by the user. We point out that α cannot be arbitrarily selected. Indeed, looking at the *modified shear energy* (see (25.37))

$$\frac{\lambda \alpha}{2} \int_{\Omega} |(\nabla v_h - \eta_h)|^2 + \frac{\lambda(t^{-2} - \alpha)}{2} \int_{\Omega} |R_h(\nabla v_h - \eta_h)|^2,$$

one easily realizes the following.

- If α is “too small,” we are essentially reducing the whole shear energy. Hence, spurious modes will likely occur.
- If α is “too large” (i.e., close to t^{-2}), we are essentially neglecting the effect of the reduction operator. Hence, the shear locking phenomenon will likely occur.

However, some numerical evidences reveal that the *PSRI* technique is quite robust with respect to the parameter choice (see [ChLo95] and [AuLo99]). Therefore, one does not expect dramatic consequences even though one misses the “optimal” α (whatever “optimal” means in this context). We finally remark that one could set α varying from element to element, also selecting the *local* value $\alpha(T)$ as a function of the size of the current element T . This kind of choice sometimes leads to an improved performance of the scheme at hand. For more details on this point, as well as other similar techniques inspired by the *least-squares augmented formulations*, see [ChSt98] and [St95], for instance.

25.3.5 Non-Conforming Elements

Recently, the development of *discontinuous Galerkin (DG)* methods for elliptic problems have also suggested new approaches to the Reissner–Mindlin plate problems: non-conforming and DG-based elements have been designed and analyzed (see [ABM], [BrMa03], and [Mi01]). We however remark that a non-conforming element has already been presented in connection with the Arnold–Falk scheme (see Section 25.3.2), but only for the approximation of the vertical displacements.

We here focus on a “*fully*” *non-conforming* low-order triangular element stemming from the following choices, as proposed, analyzed, and numerically tested in [Lo05] and [CLM06].

- Θ_h and W_h : all the kinematic variables are approximated by means of locally linear functions, which are continuous across adjacent elements *at the edge mid-points* (*non-conforming P_1 element*, see Figure 25.11).
- $R_h = P_0$, the L^2 -projection operator on the piecewise constant functions. Notice that $P_0(\nabla_h v_h) = \nabla_h v_h$ for every $v_h \in W_h$, which prevents the occurrence of spurious modes.

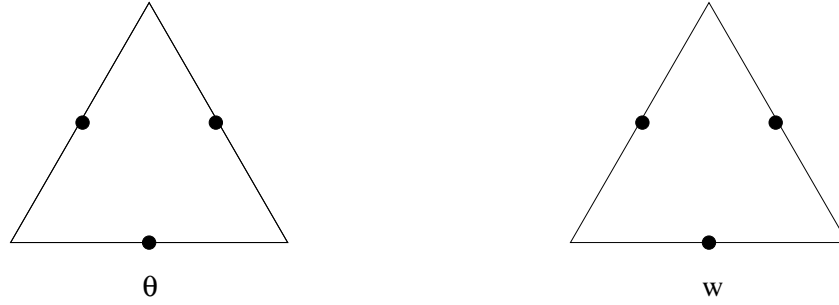


Fig. 25.11. Non-conforming element.

Then, the discrete problem reads

$$\begin{cases} \text{Find } (\theta_h, w_h) \in \Theta_h \times W_h \text{ which minimizes} \\ E_{h,t}(\eta_h, v_h) = \frac{1}{2}a_h(\eta_h, \eta_h) + \frac{\lambda t^{-2}}{2} \int_{\Omega} |\nabla_h v_h - P_0 \eta_h|^2 - \int_{\Omega} g v_h. \end{cases} \quad (25.38)$$

Above, the bilinear form $a_h(\cdot, \cdot)$ is defined by

$$a_h(\theta, \eta) := \int_{\Omega} \mathbf{C} \varepsilon_h(\theta) : \varepsilon_h(\eta) + \sum_{e \in \mathcal{E}_h} \frac{\kappa_e}{|e|} \int_e [\theta] : [\eta], \quad (25.39)$$

where

- ε_h denotes the element-by-element symmetric gradient operator,
- $[\cdot]$ is the jump operator,
- \mathcal{E}_h is the set of edges e of \mathcal{T}_h ,
- $|e|$ denotes the length of e ,
- κ_e is a positive constant to be chosen.

We remark that κ_e must match the physical dimensions of \mathbf{C} . Therefore, a possible and highly reasonable choice is $\kappa_e = |\mathbf{C}|$, where $|\mathbf{C}|$ is some norm of \mathbf{C} . We point out that the jump term in (25.39), typical of the DG machinery, is necessary for stability: the term $\int_{\Omega} \mathbf{C} \varepsilon_h(\eta_h) : \varepsilon_h(\eta_h)$ alone is not positive definite on the non-conforming space Θ_h . In Figure 25.12 we display a rotation field $\eta_h \in \Theta_h$ such that $\int_{\Omega} \mathbf{C} \varepsilon_h(\eta_h) : \varepsilon_h(\eta_h) = 0$ but $\eta_h \neq 0$.

We also notice that the form $a_h(\cdot, \cdot)$ in (25.39) is a *strongly consistent* modification of the original form $\int_{\Omega} \mathbf{C} \varepsilon(\cdot) : \varepsilon(\cdot)$. In fact, computing $a_h(\cdot, \cdot)$ on smooth functions $\theta, \eta \in (H_0^1(\Omega))^2$, the jump term vanishes and one has $a_h(\theta, \eta) = \int_{\Omega} \mathbf{C} \varepsilon(\theta) : \varepsilon(\eta)$.

We now give a hint on why this approach gives rise to a locking-free scheme. For $t \rightarrow 0$, problem (25.38) becomes

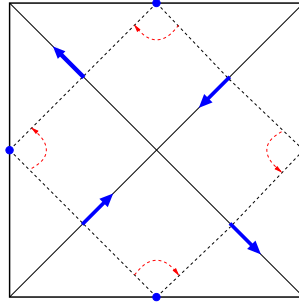


Fig. 25.12. Rotational spurious mode.

$$\begin{cases} \text{Find } (\theta_h^0, w_h^0) \in K_h \text{ which minimizes} \\ E_{h,0}(\eta_h, v_h) = \frac{1}{2} a_h(\eta_h, \eta_h) - \int_{\Omega} g v_h, \end{cases} \quad (25.40)$$

where

$$K_h = \{(\eta_h, v_h) \in \Theta_h \times W_h : \nabla_h v_h - P_0 \eta_h = 0\}. \quad (25.41)$$

Recalling the mid-point integration formula, one deduces from (25.41) that $(\eta_h, v_h) \in K_h$ means that the constraint $\nabla_h v_h = \eta_h$ is imposed *only* at the triangle barycenters, and *not everywhere*. Together with the continuity requirement only at the edge mid-points (see Figure 25.11), this makes the space K_h large enough to approximate the continuous space K defined in (25.7).

References

- [ArBr93] Arnold, D.N., Brezzi, F.: Some new elements for the Reissner–Mindlin plate model, in *Boundary Value Problems for Partial Differential Equations and Applications*, Lions, J.-L., Baiocchi, C. (eds.), Masson, Paris (1993), 287–292.
- [ABM] Arnold, D.N., Brezzi, F., Marini, L.D.: A family of discontinuous Galerkin finite elements for the Reissner–Mindlin plate. *J. Sci. Comp.* **22**, 25–45 (2005).
- [ArFa89] Arnold, D.N., Falk, R.S.: A uniformly accurate finite element method for the Reissner–Mindlin plate. *SIAM J. Numer. Anal.*, **26**, 1276–1290 (1989).
- [AuLo99] Auricchio, F., Lovadina, C.: Partial selective reduced integration schemes and kinematically linked interpolations for plate bending problems. *Math. Models Methods Appl. Sci.*, **9**, 693–722 (1999).
- [AuLo01] Auricchio, F., Lovadina, C.: Analysis of kinematic linked interpolation methods for Reissner–Mindlin plate problems. *Comput. Methods Appl. Mech. Engrg.*, **190**, 18–19 (2001).
- [AuTa94] Auricchio, F., Taylor, R.L.: A shear deformable plate element with an exact thin limit. *Comput. Methods Appl. Mech. Engrg.*, **118**, 393–412 (1994).

- [Ba95] Bathe, K.J.: *Finite Element Procedures*, Englewood Cliffs, NJ (1995).
- [BBF89] Brezzi, F., Bathe, K.J., Fortin, M.: Mixed-interpolated elements for Reissner–Mindlin plates. *Internat. J. Numer. Methods Engrg.*, **28**, 1787–1801 (1989).
- [BrFo86] Brezzi, F., Fortin, M.: Numerical approximation of Mindlin–Reissner plates. *Math. Comput.*, **47**, 151–158 (1986).
- [BrFo91] Brezzi, F., Fortin, M.: *Mixed and Hybrid Finite Element Methods*, Springer, New York (1991).
- [BFS91] Brezzi, F., Fortin, M., Stenberg, R.: Error analysis of mixed-interpolated elements for Reissner–Mindlin plates. *Math. Models Methods Appl. Sci.*, **1**, 125–151 (1991).
- [BrMa03] Brezzi, F., Marini, L.D.: A nonconforming element for the Reissner–Mindlin plate. *Computers and Structures*, **81**, 515–522 (2003).
- [ChSt98] Chapelle, D., Stenberg, R.: An optimal low-order locking-free finite element method for Reissner–Mindlin plates. *Math. Models Methods Appl. Sci.*, **8**, 407–430 (1998).
- [ChPa94] Chenais, D., Paumier, J.-C.: On the locking phenomenon for a class of elliptic problems. *Numer. Math.*, **67**, 427–440 (1994).
- [ChLo95] Chinosi, C., Lovadina, C.: Numerical analysis of some mixed finite element methods for Reissner–Mindlin plates. *Comput. Mech.*, **16**, 36–44 (1995).
- [CLM06] Chinosi, C., Lovadina, C., Marini, L.D.: Nonconforming locking-free finite elements for Reissner–Mindlin plates. *Comput. Methods Appl. Mech. Engrg.*, **195**, 3448–3460 (2006).
- [Ci78] Ciarlet, P.G.: *The Finite Element Method for Elliptic Problems*, North-Holland, Amsterdam (1978).
- [Du92] Duran, R., Liberman, E.: On mixed finite element methods for the Reissner–Mindlin plate model. *Math. Comput.*, **58**, 561–573 (1992).
- [Hu87] Hughes, T.J.R.: *The Finite Element Method*, Englewood Cliffs, NJ (1987).
- [Lo96] Lovadina, C.: A new class of mixed finite element methods for Reissner–Mindlin plates. *SIAM J. Numer. Anal.*, **33**, 2457–2467 (1996).
- [Lo98] Lovadina, C.: Analysis of a mixed finite element method for the Reissner–Mindlin plate problems. *Comput. Methods Appl. Mech. Engrg.*, **163**, 71–85 (1998).
- [Lo05] Lovadina, C.: A low-order nonconforming finite element for Reissner–Mindlin plates. *SIAM J. Numer. Anal.*, **42**, 2688–2705 (2005).
- [Ly00] Lyly, M.: On the connection between some linear triangular Reissner–Mindlin plate bending elements. *Numer. Math.*, **85**, 77–107 (2000).
- [Mi01] Ming, P., Shi, Z.-C.: Nonconforming rotated Q_1 element for Reissner–Mindlin plate. *Math. Models Methods Appl. Sci.*, **11**, 1311–1342 (2001).
- [SaPa92] Sanchez-Palencia, E.: Asymptotic and spectral properties of a class of singular-stiff problems. *J. Math. Pures Appl.*, **71**, 379–406 (1992).
- [St95] Stenberg, R.: A new finite element formulation for the plate bending problem, in *Asymptotic Methods for Elastic Structures*, Ciarlet, P.G., Trabucho, L., Viaño, J. (eds.). de Gruyter (1995), 209–221.
- [TeHu85] Tessler, A., Hughes, T.J.R.: A three-node Mindlin plate element with improved transverse shear. *Comput. Methods Appl. Mech. Engrg.*, **50**, 71–101 (1985).